J Mol Model (2005) 11: 293–300
DOI 10.1007/s00894-005-0266-5

ORIGINAL PAPER

Bogdan Kuchta · Lucyna Firlej · Guillaume Maurin

Modeling of adsorption in nanopores

Received: 1 November 2004 / Accepted: 17 January 2005 / Published online: 12 May 2005

Abstract Adsorption in nonporous materials has been studied using Grand Canonical Monte Carlo simulations. We discuss three types of materials: (a) a model of cylindrical pores with smooth walls, representing MCM-41 like materials, (b) a model of cylindrical pores with regular structured walls (model of carbon nanotubes) and (c) a material with crystalline wall structure (zeolites). Typical problems related to the stability of adsorbed layers have been analyzed. We have shown that the mechanism of adsorption is strongly dependent on the structure of the pore walls. In the case of amorphous walls it may lead to metastable configurations. In nanotubes, the ordered corrugation structure of walls determines the low temperature structure of the adsorbed system. In 3D ordered porous system, such as zeolites, the mechanism of adsorption is mostly determined by characteristic sites of adsorption.

Keywords Adsorption mechanism · Nanopores · Monte Carlo simulations · Atom–wall interaction

Introduction

Adsorption is one of the many techniques used to characterize porous materials. At the same time, the process of adsorption is directly involved in various applications. Numerous examples [1] show a variety of mechanisms of in-pore adsorption that depend on many parameters such as thermodynamic conditions, surface structures, interactions between the adsorbed particles (adsorbate–adsorbate) and between the surface and the particles (adsorbate–adsorbent). The first theories of adsorption (e.g., Langmuir theory [2, 3]) as well as the most frequently used models (e.g., BET model [4]) ignored the lateral interaction between particles of adsorbate and explained the adsorption isotherms using only vertical components of the interaction. Although this seems to be a rather important constraint leading to an underestimation of monolayer adsorption [5], the BET isotherms are still the most frequently used in the experimental adsorption data analysis.

Applications of computer modeling methods to study adsorption in pores show how strongly adsorption is dependent on the interaction model. A lot of the work was performed using simple models with regular shaped pores and smooth walls. However, there are relatively few real adsorbents that conform exactly to the regular (cylindrical and slit) shapes. A strong influence of the pore shape on the thermodynamics of systems in confined geometry is well known [2]. It is known that the discrete structure of walls must play a role in the adsorption mechanism, especially in ultra-micropores where the average diameter exceeds only few times the size of the adsorbate.

It has been known for a long time that adsorption isotherms on smooth surface (that is, with the delta-like distribution of adsorption sites), at relatively low temperatures, can show step-wise behavior. Methane adsorption on MgO is a typical example [6]. Similar stepwise adsorption has been found for methane in nanoporous graphite [7]. Oxygen adsorbed on graphite exhibits layering transitions, between crystalline layers below 43.8 K and liquid like at higher temperatures [8]. Argon exhibits a ''re-entrant'' layering behavior [8], in which layer-wise transitions disappear near 69 K and then reappear around 74 K. In all these situations, adsorbing gas tends to complete each successive layer before beginning the next one. In addition, the steps in these isotherms can be very sharp, suggesting a possible

B. Kuchta (✉) · G. Maurin
Laboratoire des Matériaux Divises, Revêtement,
Electrocéramiques (MADIREL),
Université de Provence,
Centre de Saint-Jérôme,
13397 Marseille, France
E-mail: Bogdan.kuchta@up.univ-mrs.fr

L. Firlej
Groupe de Dynamique des Phases Condensées (GDPC),
Université Montpellier II,
34095 Montpellier, France

interpretation as phase transition type behavior. When the wall is structured, that means corrugated or amorphous (disordered), the adsorption sites become non-equivalent. In such cases, the adsorption may lose its step-wise character when the sites' distribution width is small compared to the total atom–wall energy. The situations discussed in this paper correspond to three distinct cases, from amorphous to crystalline ordered pore walls.

The microscopic mechanism of transitions in confined geometry has been studied using theoretical methods and computer simulation techniques [6]. Layering transitions have been found in cylindrical pores of diameter 14σ (σ is the Lennard-Jones (LJ) parameter) [9], in models of carbon nanotubes with nitrogen and argon as adsorbed atoms [10] and in slit pores (adsorption of methane [8]). Experimentally, the microscopic mechanism of adsorption is always "hidden" behind the macroscopic measurement. The "time factor" is very important here. The computer simulations offer much shorter times than real macroscopic observations. This means that the ergodic hypothesis is not always satisfied because the system may be trapped in a metastable situation. This factor is important in pore geometries where the hysteresis of adsorption (corresponding to capillary condensation phenomenon) is observed at a macroscopic scale. We will show that this phenomenon is also present at the microscopic level.

In this paper we analyze the influence of the wall structure on mechanism of adsorption using the Grand Canonical Monte Carlo (GCMC) simulation method. We discuss three types of system, starting from cylindrical pore geometry, with nanometric diameters and amorphous walls (a model of MCM-41 material), through cylindrical pores with well defined structures of walls (carbon nanotubes), up to the crystalline structures of zeolites.

Materials and methods

The conventional grand canonical MC ensemble was applied to simulate adsorption in pores. The simulation box (with periodic boundary conditions along the periodic directions) was assumed to be in equilibrium with the bulk gas, which obeyed the ideal gas law. This allowed us to use the external gas pressure as the thermodynamic parameter instead of the potential [11]. Trial moves included the translations of atoms, insertion of new atoms and removal of existing ones. The studied systems typically contained up to 1300 adsorbed atoms or molecules in the box. Typical runs consisted of the minimum number of 10^6 MC steps (per atom). The main results were extracted from the previously equilibrated runs.

The simulation conditions of amorphous pores were defined in the same way as in our previous papers [12, 13] including the applied interaction parameters [14]. The adsorbed gases were krypton and argon in smooth pores that were used to model the MCM-41 material, of diameter 4 nm.

The atom–nanotube wall interactions were computed by a pair-wise summation of classical LJ 6–12 potential (with the LJ parameters for the atom–C interaction obtained from Lorentz–Berthelot mixing rules) [15]. Using this potential, the 3D grid of gas-nanotube surface potential was precalculated and implemented into MC code, to account for the atomic roughness of carbon nanotubes. The results showed in this paper were obtained for (10, 10) armchair single wall tube nanotube, of a diameter of 13.56 Å .

Our flexible zeolite framework is treated as semi-ionic with partial charges. Here we focus our attention on Na^+ -mordenite characterized by the ideal composition of the unit cell $Na_8Al_8Si_{40}O_{96}$, nH_2O with n ranging from 0 (dehydrated state) to 24 (totally hydrated state). Its structure is orthorhombic (*Cmcm*) with unit cell parameters $a = 18.1$ Å, $b = 20.5$ Å and $c = 7.5$ Å[5] . Polarizability is taken into account by a shell model for the oxygen atoms [16]. The potential developed by de Leeuw et al. [17] is selected for modeling polarizable water molecules. The interactions between water and both extra-framework cations and oxygen of the zeolite framework are described by LJ and Buckingham potentials [18]. Ewald summation is used to calculate the coulombic interactions and a cut off at 16 Å for the short range contributions. We use the various energy minimization techniques available in GULP (General Utility Lattice Program) [19]. We built the structure of the fully hydrated Na^+ -mordenite by step-wise addition of the water molecules into the dehydrated mordenite.

Results

Nanopores with amorphous walls

The cylindrical, nonconnected pores are relatively simple systems. However, even such simple geometry may exhibit very intricate properties depending on interactions and geometry of the wall structure. Let us start with the simplest situation of smooth, ideal walls. The argon and krypton isotherms of adsorption in such pores, at 77 K, are shown in Fig. 1. Obviously, they are very different. The only similarity between them is the step-wise form and the low-pressure region (below the first layer formation) where adsorbed atoms form a very low-density structure (two-dimensional analog of the gas state). At the same time, the krypton isotherm exhibits very sharp formation of the first layer, whereas argon shows a more continuous increase in the number of adsorbed atoms. It is important to emphasize that the main source of this difference is the state of the adsorbed layer: at 77 K argon form liquid layers and krypton is solid. This comparison shows that the mechanism of layering transition is a complicated phenomenon that depends strongly on the relative strength of the adsorbent–adsorbate and adsorbent–adsorbent particles interac-

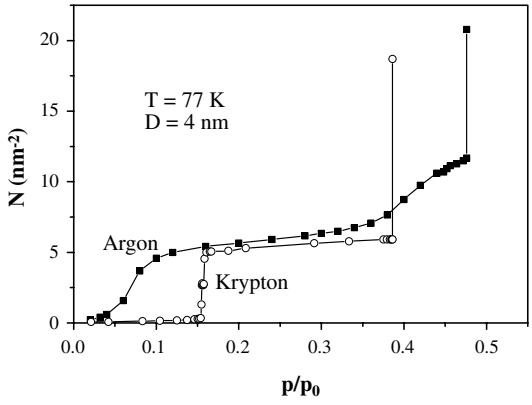

Fig. 1 The isotherms of adsorption of Kr and Ar in the smooth wall pore of diameter 4 nm at 77 K. Number of atoms N gives the average number of adsorbed atom per nm^2 of the pore wall. The last reported points correspond to the capillary condensation. p/p_0 is the reduced pressure, where p_0 is the saturation pressure at 77 K

tions. However, the pressure of the layering transition is a continuous function of the strength of the atom–wall interaction (Fig. 2). As could be expected, a weaker interaction leads to higher transition pressure. In the limit of no atom–wall interaction (hard walls), the layering transition must disappear. However, a weaker interaction also reduces the range of pressure where the first layer is stable. As it can be seen from Fig. 2, for krypton, the difference between the first layer formation and capillary condensation disappears below the saturation pressure. In this situation, only capillary condensation would be observed given the weak atom–wall interaction. The formation of the first layer may be interpreted as an analog of the 3D gas–solid phase transition. In krypton, at 77 K, it is very discontinuous. In our Monte Carlo box we observed that the system jumps between gas-like (2D) and solid-like (adsorbed layer) phases, in a very narrow range of pressures. This bimodal behavior is well pronounced and easily observed from instantaneous fluctuations of the number of adsorbed atoms and from the energy fluctuation distribution (Fig. 3). It seems that the free energy barrier between these two states is negligible in these thermodynamic conditions. Remembering that the size of our Monte Carlo system is limited, it is impossible to decide whether this is like a I-order or II-order transition. However, no hysteresis was observed. A stronger atom–wall interaction not only shifts the pressure of the transition toward lower pressure but also makes it more discontinuous. The mechanism of this phase transition will be discussed in separate paper [20]. A similar layering transition in argon, at the same temperature of 77 K, shows a different mechanism. This appears in a gradual and continuous manner, in a finite range of pressures. There is no bimodal behavior, as observed in krypton, but still the intermediate states between the gas-like phase and the full layer structure are characterized by much higher fluctuations than the gas and monolayer structures.

However, the experimental isotherms of adsorption of krypton and argon in MCM-41 show a steep initial rise at low pressure, which is not observed in simulations on smooth walls [5]. The reason for that is the hetero-

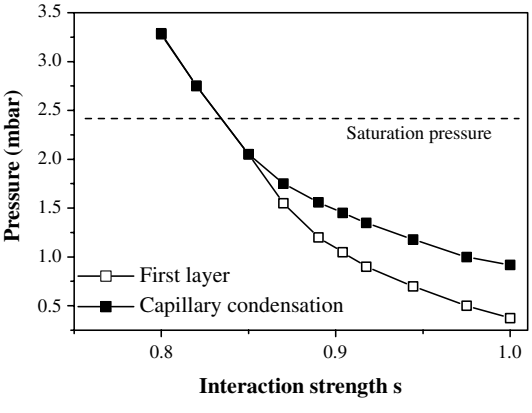

Fig. 2 The pressure of the layering transition (first layer formation) and capillary condensation of krypton as a function of the strength parameter s (s is the factor which defines the effective interaction, that is, effective Lennard-Jones parameter of the atom–wall interaction: $\epsilon_{eff} = s\epsilon$. The parameter σ is unchanged)

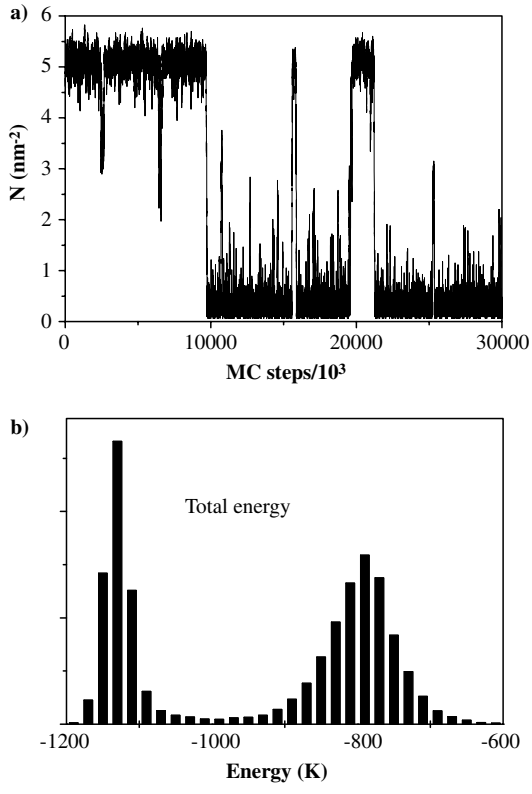

Fig. 3 Adsorbed atoms and energy fluctuations at the pressure of the first layer formation of krypton atoms: **(a)** instantaneous numbers of adsorbed atoms (per nm^2 of the pore wall) as a function of the time of simulation (Monte Carlo steps) observed in a relatively long run, **(b)** the bimodal distribution of the energy fluctuations is a consequence of the behavior of the systems as shown in **(a)**

geneity of real walls, as discussed in previous papers [12, 13]. The main factor seems to be a micropore structure of heterogeneous walls where strong adsorption is present even at low pressure. The strong wall corrugation has some additional effects on the microscopic states in equilibrium and on the mechanism of the transformations. During the simulation runs we have observed different metastable configurations that existed as intermediate states of the system. As an example, we present the simulated fluctuations of the number of atoms in the MC box when the system is undergoing the capillary condensation (Fig. 4). It clearly shows an intermediate, metastable state before the pore condensation is completed and consists of a formation of the second layer, which exists only within limited time of simulation. Instead of stabilizing it, the system undergoes a transformation into the condensed phase (fully filled pore).

Carbon nanotubes: cylindrical pores with ordered wall structure

Carbon nanotubes are other examples of systems with nonconnected cylindrical pores. In this case the pore walls, formed by cylindrical graphene sheets, are regularly structured. The atomic structure of graphite introduces corrugation of the atom–wall potential and, as a consequence, heterogeneity of the adsorption sites. Its symmetry, nearly hexagonal, is characteristic for graphite but deformed due to the cylindrical symmetry and reproduces the geometry of the nanotube. In the case of ''armchair'' type of nanotubes (Fig. 5), the energy of the saddle points along the tube axis are slightly lower than the others. This difference is important enough to affect the structures of adlayers at low temperatures and influences the fluctuations in the system at higher temperatures.

At the same time, most of the reported computer modeling studies of adsorption in carbon nanotubes neglect systematically the real atomic structure of the tube wall [21–28]. Instead, it is assumed that carbon atoms are smeared out on a smooth cylinder with a homogeneous carbon density of 0.381 atoms/Å^2 . However, it has been shown that the corrugation of the substrate, even if it constitutes a small fraction of the total energy of the system, is essential in determining the structure of the adsorbed layers [29, 30].

In the case of nanotubes, the adsorbate structure tries to match the carbon structure as much as interatomic interaction will allow. When the density of adsorbed atom is small and the interatomic interactions are not important, the atoms occupy the adsorption sites located in front of the centers of the wall hexagons. However, when the first layer is nearly formed, the competition between atom–atom and atom–wall interactions defines the final structure. At low temperatures, where the layer is solid, the adsorbed atoms form structures that are more or less commensurate with the nanotube symmetry. If the atom–atom equilibrium distance is comparable with a distance between those minima, the registered, commensurate structure may be formed. Otherwise, different forms of incommensurate structures are observed. Figure 6 presents some examples.

Another manifestation of the influence of the regular wall structure on properties of the adsorbed system appears at temperatures close to the melting/freezing transition. Because of the cylindrically deformed hexagonal symmetry described above, in some directions the saddle points between two carbon atoms are not equivalent. When the adsorbed atoms have enough energy to overcome the lowest energy barriers between the closest adsorption centers, a preferred one dimensional translational fluctuation occurs between them. This leads to the spectacular effect of one dimensional melting (Fig. 6b). One may expect that the direction of these one dimensional fluctuations will be dependent on the chirality of a nanotube. We are in the process of verifying this behavior.

The corrugation of the wall may also be responsible for a metastable behavior of the adsorbed system, in a similar way that it was observed in the case of heterogeneous (amorphous) pore walls. For example, at low temperature, it leads to metastable structures of adsorbed layers, different during the adsorption and

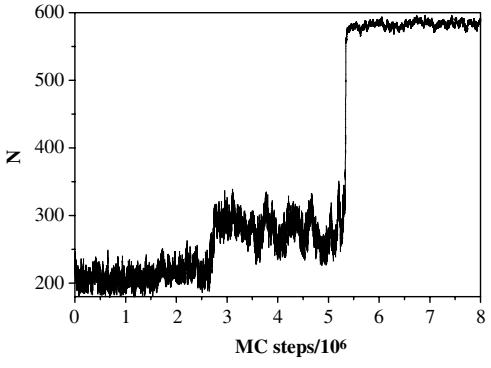

Fig. 4 The fluctuations of the number of atoms in the simulation box as a function of the Monte Carlo steps, at the capillary condensation pressure. The pore walls are disordered and modeled by a wide distribution of adsorption sites

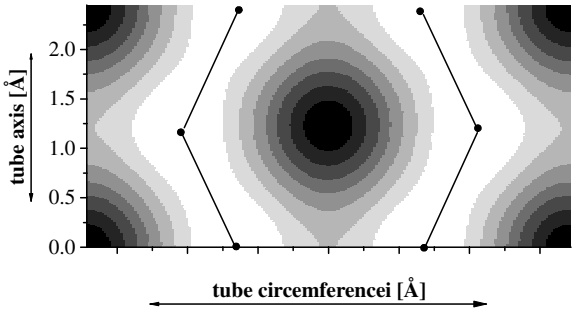

Fig. 5 Interaction of the He atom with the wall of a ''armchair'' nanotube. The energy minima correspond to the *black* areas

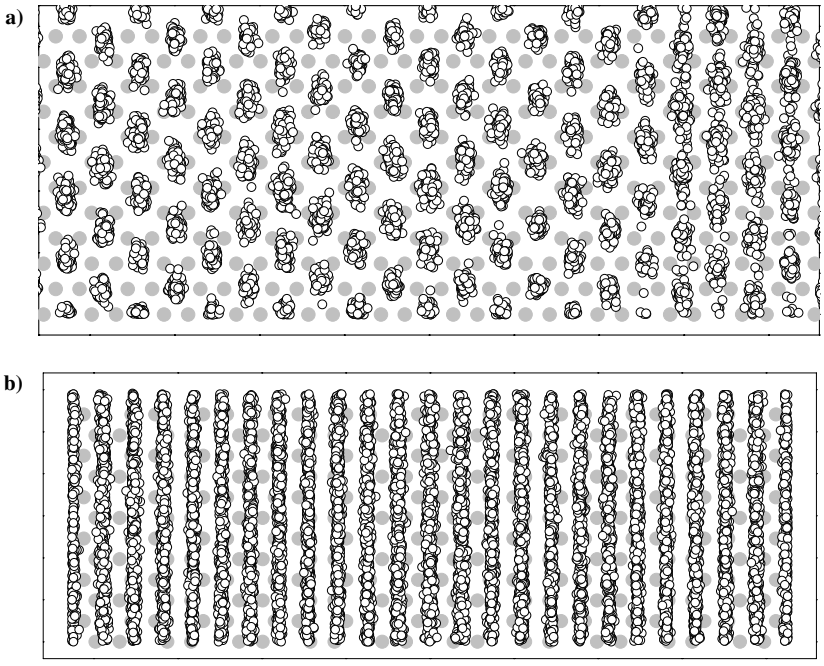

Fig. 6 Instantaneous structures of He layers adsorbed on carbon nanotube: **(a)** solid layer, $T = 0.5$ K, **(b)** liquid layer, $T = 7$ K. The graphs have been presented as unfolded layers of graphite (represented by *gray closed circles*) and adsorbed layer instantaneous configurations (*open black circles*)

desorption processes. Generally, the problem of metastability has many aspects that go beyond the frame of this paper.

Zeolites: network of pores in ordered material

More complex systems of pores, consisting of channels and cages, are represented by the aluminosilicate framework of zeolites. Zeolites are involved in a large domain of chemical science and technology including catalytic [31] and separation processes, gas storage and ion exchange [32, 33]. The anionic character of their lattice (due to the substitution of silicon by aluminum) is neutralized by exchangeable cations which are located in well defined surface sites surrounded by oxygen atoms of the framework [34]. Here we focus our discussion on Na^+ -mordenite characterized by the ideal composition of the unit cell $Na_8Al_8Si_{40}O_{96}$. The framework has a porous structure which consists of main channels having a slightly elliptical cross section with 12 TO_4 tetrahedron units (T = Si, Al) and connected with small side channels consisting of 8 TO_4 (Fig. 7). The unit cell considered in our simulation was built by substituting silicon atoms by aluminum atoms in order to satisfy the Lowenstein's rule which prohibits Al–O–Al arrangement. Such a selected configuration reproduces well the Si– nAl ($n = 0$, 1, 2, 3) distribution obtained by [29] Si NMR spectra.

Water plays a key role in many applications involving adsorption and, more particularly, in ion-exchange carried out in aqueous solutions [35]. In this latter case, it is well known that water improves the efficiency of this process by coordinating the cations and hence increasing their mobility [36, 37]. Computer simulations may provide a microscopic description of the effect of water on the behavior of the exchangeable cations, modeling the whole hydration process, from dehydrated to the totally hydrated state (containing 24 water molecules per unit cell). In the dehydrated state, the extra-framework cations are located half in the main channels (sites IV and VI) and half in the small channels (site I) (Fig. 8). This result is in good agreement with experimental X-ray diffraction data [34, 37].

The simulated water adsorption occurs as follows. The first two water molecules do not influence strongly the extra-framework cations and their positions are not affected by the presence of the adsorbed water. For $n = 3$, 6, 7 and 11 water molecules per unit cell the cations of the main channels are progressively extracted from their initial sites. No further evolution is observed between $n = 11$ and $n = 24$ hydration levels. At the same time, the cations in the small channels are only slightly perturbed by water molecules occupying neighboring side pockets and remain trapped in the same initial positions (independently of the hydration level). These two different types of cation behaviors are summarized in Fig. 9,which shows the fully hydrated structure of Na^+ -mordenite.

These results are in good qualitative agreement with experiment [38] which predicts that the population of site I remains constant whatever the H_2O content is, and that the occupations of sites IV and VI dramatically decrease in the range 3.2–8.7 H_2O per unit cell. This agreement is achieved by the realistic modeling of the crystalline pore wall structure which introduces a distribution of the adsorption sites, very regular and defined by the symmetry of the periodic network. However, this time their population depends also on the presence of other species in the pore.

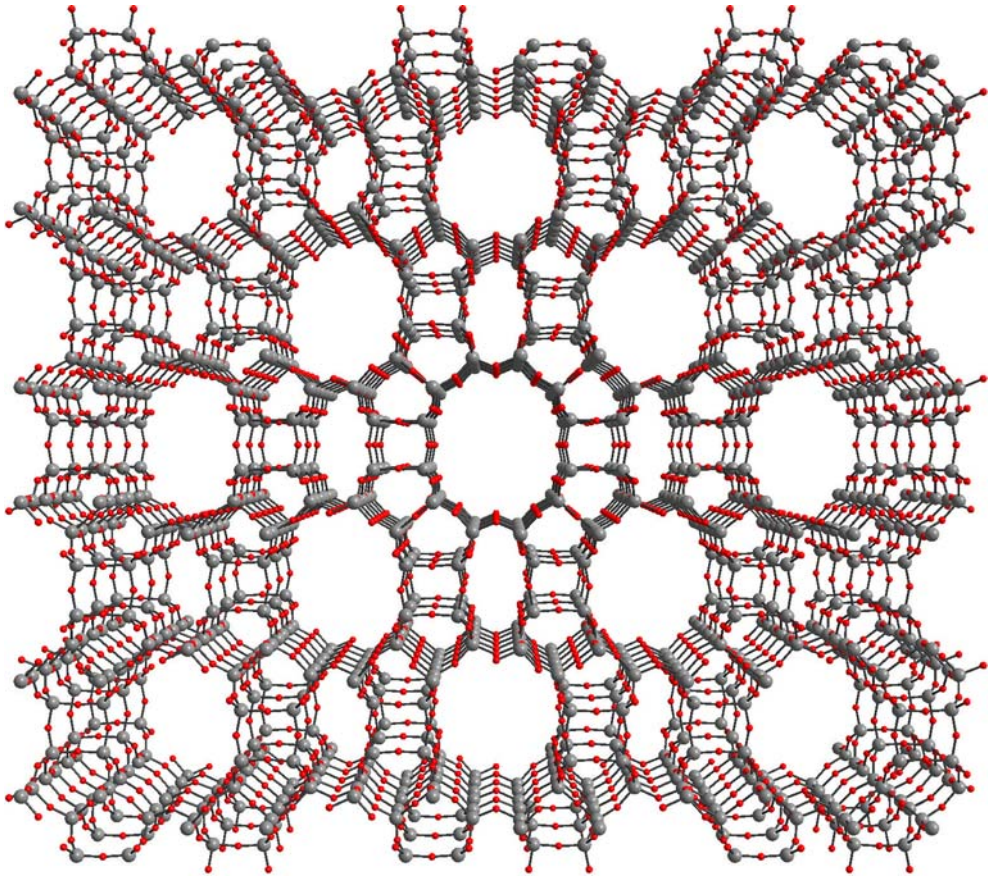

Fig. 7 Representation of the mordenite framework

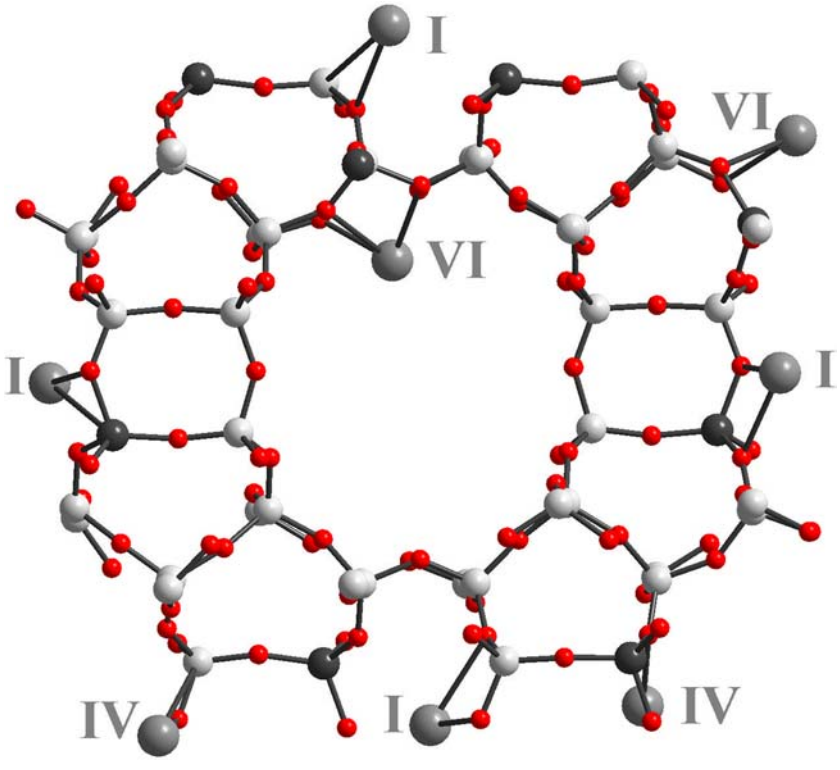

Fig. 8 Distribution of the extra-framework cations in the dehydrated structure among the three distinct crystallographic cation sites I, IV and VI

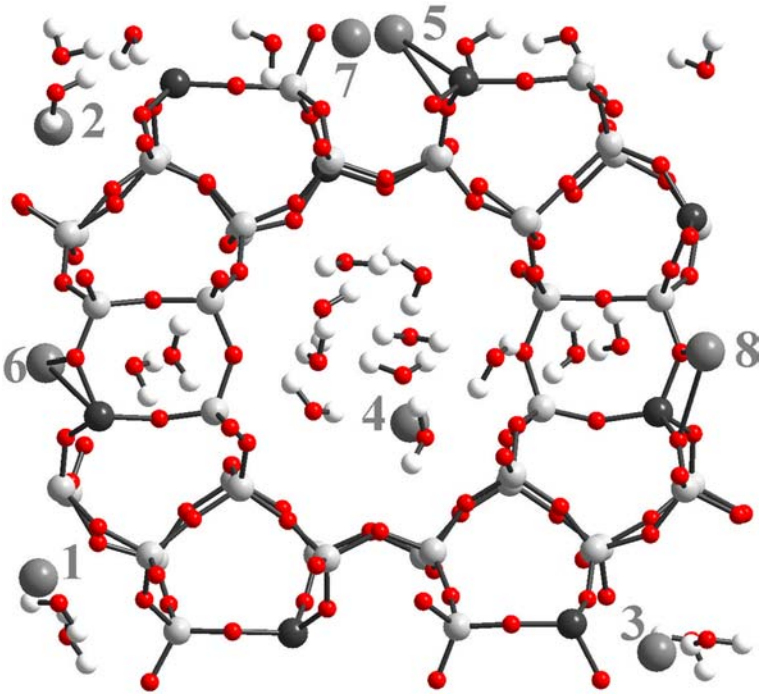

Fig. 9 Representation of the fully hydrated Na^+ -mordenite. The cations in the main channels (1, 2, 3, 4) are de-trapped from their initial sites, whereas the cations in the small channels (5, 6, 7, 8) are only slightly shifted

Conclusions

Three different adsorbing systems have been presented in this paper. Their chemical nature is different and they possess different structures. As a consequence, the adsorbed atoms or molecules are exposed to different structures of the adsorbing walls, with different strengths of the adsorbate–adsorbent interactions. The effect of such variety of the adsorbing conditions is observed experimentally, on the macroscopic level (e.g., from different shapes of the isotherms of adsorption). However, their microscopic nature is accessible only in computer modeling. Examples have been presented in this paper: bimodal behavior of adsorption on a smooth surface of silica-based pores, formation of incommensurate structures on carbon nanotubes and the extraction of the cations from their crystallographic sites in zeolites when water is adsorbed.

The most important characteristic of an adsorbing system, from the point of view of its microscopic properties, is the structure of the adsorbent. It determines the state of the first adsorbed layer and, indirectly, it affects the configurations of subsequent layers. More ordered walls induce a step-wise formation of the monolayer. More disordered situations are responsible for a continuous adsorption, often very rapid at low pressures due to a micropore size distribution. Additionally, at low temperatures, a regular structure of walls strongly affects the adsorbate configuration.

Metastability in adsorbed system is observed on the macroscopic level as hysteresis, measured during the capillary condensation. However, the computer simulations also reveal the existence of metastability on the microscopic level. By ''microscopic'' metastability we understand a metastable state which is observed in simulations during limited time, usually, as an intermediate state between two equilibrium configurations. The character of the distribution of adsorption sites is the direct factor defining this ''microscopic'' metastability. We observed such situations in the case of gases adsorbed on heterogeneous walls of both regular and amorphous structures. This phenomenon and its consequences require more studies.

References

1. Rouquerol F, Rouquerol F, Sing K (1999) Adsorption by powders and porous solids. Academic, London
2. Langmuir I (1916) Phys Rev 8:149–176
3. Langmuir I (1918) J Am Chem Soc 40:1361–1403
4. Brunauer S, Emmet PH, Teller E (1938) J Am Chem Soc 60:309–329
5. Bienfait M, Zeppenfeld P, Gay JM, Palmari JP (1990) Surf Sci 22:327–338
6. Gelb LD, Gubbins KE, Radhakrishnan R, Sliwinska-Bartkowiak M (1999) Rep Prog Phys 62:1573–1659
7. Larese JZ, Harada M, Passell L, Krim J, Satija S (1988) Phys Rev B 37:4735–4742
8. Youn HS, Hess GB (1990) Phys Rev Lett 64:443–446
9. Peterson BK, Zhang QH, Larese JZ (1990) J Chem Phys 93:679–685
10. Maddox MW, Gubbins K E (1997) J Chem Phys 107:9659–9667
11. Frenkel D, Smit B (1996) Understanding molecular simulations. Academic, London
12. Kuchta B, Llewellyn P, Denoyel R, Firlej L (2003) J Low Temp Phys 29:880–882
13. Kuchta B, Llewellyn P, Denoyel R, Firlej L (2004) Colloids Surf A 241:137–142
14. Siperstein FR, Gubbins KE (2002) In: Rodrigues-Reinoso F, McEnaney B, Rouquerol J, Unger K (eds) Characterizations of porous solids VI. Elsevier, Amsterdam, pp 647–654

15. Stan G, Crespi VH, Cole MW, Boninsegni M (1998) J Low Temp Phys 113:447–452
16. Jackson RA, Catlow CRA (1988) Mol Simul 1:207–224
17. Manon Higgins F, de Leeuw NH, Parker P (2002) J Mater Chem 12:124–131
18. Maurin G, Bell R, Devautour S, Henn F, Giuntini JC (2004) J Phys Chem B 108:3739–3745
19. Gale JD (1997) J Chem Soc Faraday Trans 93:629–637
20. Kuchta B, Firlej L (2005) J Low Temp Phys (in press)
21. Calbi MM, Cole MW (2002) Phys Rev B 66:115413–115424
22. Calbi MM, Gatica SM, Bojan MJ, Cole MW (2001) J Chem Phys 115:9975–9981
23. Gatica SM, Bojan MJ, Stan G, Cole MW (2001) J Chem Phys 114:3765–3769
24. Ščaron iber A (2002) Phys Rev B 66:205406–205411
25. Calbi MM, Cole MW, Gatica SM, Bojan MJ, Stan G (2001) Rev Modern Phys 73:857–865
26. Stan G, Bojan MJ, Curtarolo S, Gatica SM, Cole MW (2000) Phys Rev B 62:2173–2180
27. Gordillo MC, Boronat J, Casulleras J (2000) Phys Rev B 61:R878–R881
28. Stan G, Crespi VH, Cole MW, Bonisegni M (1998) J Low Temp Phys 113:447–452
29. Etters RD, Flenner E, Kuchta B, Firlej L, Przydrozny W (2001) J Low Temp Phys 122:121–128
30. Firlej L, Kuchta B, Etters RD, Przydrozny W, Flenner E (2001) J Low Temp Phys 122:171–177
31. Corma A (2003) J Catal 216:298–312
32. Ackley MW, Rege SU, Saxena H (2003) Microporous Mesoporous Mater 61:25–42
33. Froment GF, Jacobs PA (2000) Top Catal 13:444–447
34. Mortier WJ (1982) Compilation of extra-framework sites in Zeolites. Butterworth, Guildford
35. Pissis P, Daoukaki-Diamanti D (1993) J Phys Chem Solids 54:701–709
36. Artioli G, Smith JV, Kvick A, Pluth JJ, Stahl K (1985) In: Zeolites. Elsevier, Amsterdam, pp 249–254
37. Coughlan B, Carrol WM, Mc Cann A (1977) J Chem Soc Faraday Trans 73:1612–1619
38. Devautour S, Abdoulaye A, Giuntini JC, Henn F (2001) J Phys Chem B 105:9297–9301